Multiple electron capture, excitation, and fragmentation in $C^{6+}-C_{60}$ collisions

Humberto da Silva, Jr.,[1] Javier Oller,[1] Michael Gatchell,[2] Mark H. Stockett,[2] Paul-Antoine Hervieux,[3] Lamri Adoui,[4,5] Manuel Alcamí,[1,6] Bernd A. Huber,[4] Fernando Martín,[1,6] Henrik Cederquist,[2] Henning Zettergren,[2,*] Patrick Rousseau,[4,5,†] and Sergio Díaz-Tendero[1,‡]

[1]*Departamento de Química, Módulo 13, Universidad Autónoma de Madrid, 28049 Madrid, Spain*

[2]*Department of Physics, Stockholm University, SE-106 91 Stockholm, Sweden*

[3]*IPCMS, Institut de Physique et Chimie des Matériaux de Strasbourg, CNRS and Université de Strasbourg, BP 43, F-67034 Strasbourg, France*

[4]*CIMAP, UMR 6252, CEA/CNRS/ENSICAEN/UCBN, Boulevard Henri Becquerel, BP5133, F-14070 Caen Cedex 5, France*

[5]*Université de Caen Basse-Normandie, Esplanade de la Paix, CS 14032, 14032 Caen Cedex 5, France*

[6]*Instituto Madrileño de Estudios Avanzados en Nanociencias (IMDEA-Nanociencia), Cantoblanco 28049, Madrid, Spain*

(Received 13 June 2014; published 2 September 2014)

We present experimental and theoretical results on single- and multiple-electron capture, and fragmentation, in $C^{6+} + C_{60}$ collisions at velocities in the $v_{col} = 0.05 - 0.4$ a.u. range. We use time-of-flight mass spectrometry and coincidence detection of charged fragments to separate pure target ionization from processes in which the C_{60} target is both ionized and fragmented. The coincidence technique allows us to identify different types of fragmentation processes such as $C_{60}^{q+} \rightarrow C_{58}^{q+} + C_2$ and $C_{60}^{q+} \rightarrow C_{58}^{(q-1)+} + C_2^+$. A quasimolecular approach is employed to calculate charge transfer and target excitation cross sections. First-order time-dependent perturbation and statistical methods are used to treat the postcollisional processes: the calculated rate constants for C_2 and C_2^+ emission from the excited and charged fullerene are then used to evaluate the fragmentation dynamics. We show that the target ionization cross section decreases with the induced target charge state and the impact energy. C_2 emission from C_{60}^{q+} is found to dominate when $q \leqslant 2$ while C_2^+ emission dominates when $q \geqslant 5$, in agreement with the present and previous experimental results.

DOI: 10.1103/PhysRevA.90.032701 PACS number(s): 34.50.−s, 36.40.Qv, 34.10.+x, 34.70.+e

I. INTRODUCTION

Over the past decades, fullerenes have been extensively studied by means of various excitation and ionization agents, such as photons [1–3], electrons [4–8], ions [9–24], or laser pulses [25–30]. It has been demonstrated that hot fullerene ions produced in these interactions may cool down by electron emission [29,31–33], radiative decay [34,35], or by statistical fragmentation processes [36–39]. In the last case, this is typically manifested by long sequences of neutral C_2 emissions (see, e.g., Ref. [40]). The lowest-energy dissociation channel for moderately charged fullerenes is close to 10 eV, e.g., 10.64 eV for C_{60}^+ [41,42]. Due to their high heat capacities (many degrees of freedom) internal energies well above the dissociation energy threshold are required to observe unimolecular fullerene decay on the experimental time scales: microseconds. This was unambiguously shown by the authors of Refs. [22,23], where the excitation energies of the fragmenting fullerenes in keV $H^+ + C_{60} \rightarrow H^- + C_{60}^{2+}$ and $F^{2+} + C_{60} \rightarrow F^- + C_{60}^{3+}$ collisions were measured to be $\gtrsim$50 eV. These results are important benchmark data for the validation of statistical models and molecular dynamics simulations, which have been commonly used to guide interpretations of experimental results [36,39,43–45].

Up to this date, statistical models have only been used to calculate the branching ratios for neutral fragment emissions (e.g., C_2 and C_4) from fullerene ions in low charge states [46–49]. However, it is well established that charged fragment emission becomes more important as the fullerene charge state increases due to the increase in the internal Coulomb repulsion. As a consequence, C_2^+ emission becomes a competitive processes for C_{60}^{3+} [50]. According to density functional theory calculations, C_{60}^{q+} [51] and C_{70}^{q+} [52] are thermodynamically unstable for $q > 5$, while so-called fission barriers prevent even much more highly charged systems to decay promptly [53]. Indeed, C_{60}^{q+} ions in charge states up to $q = 12$ have been observed in time-of-flight experiments [54], thus showing stability in the μs time scale.

In the laboratory, highly charged keV ions can be used to ionize fullerenes and to study the competition between neutral- and charged-fragment emissions from multiply charged C_{60}^{q+} (typically $q \sim$ 1–7) [10,11,15,24]. In such collisions, electrons may be captured at large distances with low internal fullerene heating due to nuclear and electronic stopping processes. The cross sections for charge transfer processes have been successfully rationalized with the aid of the classical over-the-barrier model treating the C_{60} molecule as a conducting sphere [11,55,56]. This model relies on the assumption that there is a (quasi) continuum of projectile capture states at the top of the barrier for electron transfer.

In the present work, we go one step further in our understanding of ionization and fragmentation of fullerene by ion projectiles in high charge states. In particular, using a similar approach as in the combined experimental and theoretical study of $He^{2+} + C_{60}$ collisions [24], we report results for the $C^{6+} + C_{60}$ collision system. We thus address the stability of the C_{60} fullerene in high charged states. Since the collision time (subfemtoseconds) is much shorter than the vibrational periods of C_{60} (approximate picoseconds),

*henning@fysik.su.se
†prousseau@ganil.fr
‡sergio.diaztendero@uam.es

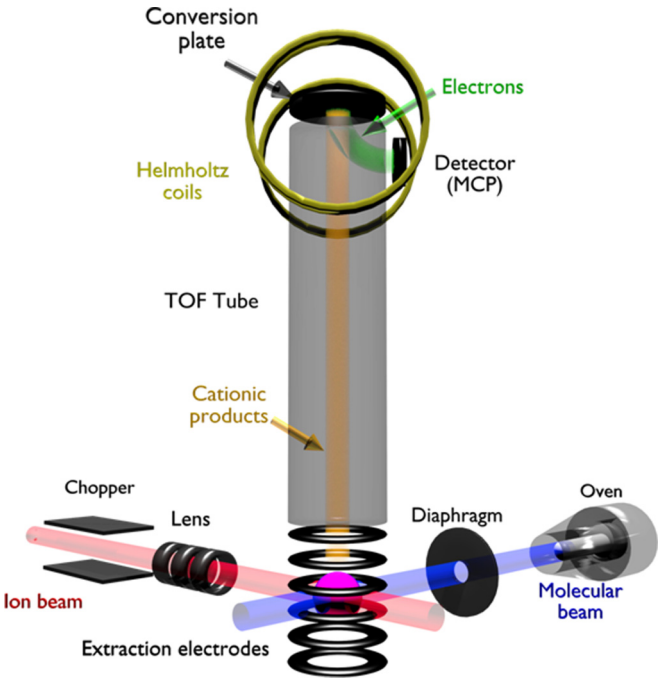

FIG. 1. (Color online) Schematic of the experimental set up (see text).

the ionization and fragmentation processes are treated separately in the theoretical calculations.

The paper is organized as follows. In Sec. II we briefly describe the present experimental mass-spectrometry technique. In Sec. III we describe how we calculate absolute charge transfer cross sections, energy transfers due to inner-shell capture processes, and branching ratios of C_2 and C_2^+ emission as functions of the fullerene charge state and internal energy. In Sec. IV we compare our calculations with the present and earlier experimental results. Finally, we summarize our main conclusions in Sec. V.

II. EXPERIMENTS

The experiments have been performed at the ARIBE facility [57], the low-energy ion beamline of GANIL in Caen, France. A schematic of the crossed beam collision device [58] is given in Fig. 1.

The C^{6+} ions are produced in an electron cyclotron resonance ion source and are accelerated to kinetic energies between 30 and 60 keV. The ion beam is mass-over-charge selected by an analyzing magnet. We use a gas of $^{13}CH_4$ to avoid the beam pollution by other multiply charged ions and we obtained a pure $^{13}C^{6+}$ beam of a few microamps after mass selection. After passing a diaphragm of 3 mm, the beam is focused by an Einzel lens into the interaction zone where it collides with a molecular beam of C_{60} fullerenes. The collision zone lies inside the extraction region of a modified linear Wiley-McLaren time-of-flight (ToF) mass spectrometer [59]. Cationic products from the target (intact fullerenes and fragments) are extracted into the mass spectrometer. To obtain a high detection efficiency of heavy particles, we use a modified Daly detector, which also allows a constant detection yield over a wide range of masses. Thus, the cations are postaccelerated at the end of the drift tube to a conversion plate and the secondary electrons emitted by the impact on the plate are guided by a weak magnetic field to a Z-stack of microchannel plates. The arrival times are digitized by a multiscaler with 1-ns resolution (FAST ComTec P7888).

The molecular beam effuses from a tube connected to a crucible filled with C_{60} powder of 99.95% purity (M.E.R. Corporation). Both parts (the tube and crucible) are resistively heated and the temperature, controlled by a thermocouple, is kept at 740 K during the experiments.

The ion beam was chopped in 500-ns pulses with a repetition rate of 4 kHz. The spectrometer extraction field is switched on within 10 ns after the beam-pulse passage through the interaction region and stays on for 8 ms. The target density and ion beam current are kept sufficiently low such that only a very small fraction of the ion beam pulses, less than 1 in 100, leads to ionization and/or fragmentation of a fullerene. This also means that the probability that there will be more than one ionization or fragmentation event per beam pulse is below 1%. The time at which the extraction voltage is switched on defines the START signal for the time of-flight measurement. Each recorded ion arrival time then gives a STOP signal and the corresponding flight time and, thus, the mass-to-charge ratio of that fragment is determined. When a fullerene evolves in such a way that at least two charged fragments are emitted, several STOP signals are recorded for the corresponding START signal. The number of charged products, i.e., the number of STOP signals is the multiplicity of the collision event. The next START signal (i.e., the next switch of the extraction pulse voltage) defines the end of the previous event. With the event-by-event list obtained, we can build spectra as a function of the multiplicity [60]. Thus, considering the high transmission and detection efficiency of the setup and its operation under single-collision conditions, the 1-STOP spectrum contains stable C_{60}^{q+} (at the μs timescale) intact fullerenes and C_n^{q+} fragments resulting from C_2 emission of C_{60}^{q+} [7]. The 2-STOPS spectrum reflects the charge-separation of C_{60}^{q+} in two charged fragments $C_n^{(q-r)+}$ and C_m^{r+} including the $(C_{58}^{(q-1)+})(C_2^+)$ ion pair which is of particular interest for the present study [20].

III. THEORETICAL METHODS

The interaction time is of the order of 10^{-14} s for ions colliding with C_{60} at velocities between 0.05 and 0.4 a.u. This is much shorter that the C_{60} vibrational period ($\sim 10^{-12}$ s). Therefore the collision is a much faster process than fragmentation and thus we can perform the theoretical treatment of these two processes separately. Here we present some details of the theoretical methods and simulations which we will later use for discussions of charge transfer, energy deposition in the fullerene, and its fragmentation.

A. Charge transfer and electronic excitation

In the simulations of the collisions, we describe the electronic structure of C_{60} by using an extension of the spherical jellium model of Puska and Nieminen [61]. Then we use the Kohn-Sham (KS) formulation of the density functional theory to describe the electronic density of the fullerene in terms

of single-particle orbitals. From these orbitals we obtain the corresponding one-electron potentials using the local-density approximation with exchange-correlation and self-interaction correction (LDAXC-SIC). The orbital-dependent potentials obtained with this method exhibit the correct asymptotic Coulomb behavior $(-1/r)$, which is crucial in this work because charge transfer and excitation occur mainly at large distances. This methodology was presented in detail in Ref. [62].

We use the potentials of the orbitals obtained for the dynamical treatment of the collision. For this, we employ the quasimolecular approach of ion-atom collisions at low energies. This approximation allows us to describe multi-electron processes in collisions with many active electrons. We solve the N_e-body problem, where N_e is the number of electrons, by means of the independent electron model (IEM) and the inclusive probability method introduced by Lüdde and Dreizler [63]. A full quantum-mechanical description in the IEM is possible because each active electron moves in the field produced by two potentials: the potential for the C^{6+} projectile and the calculated (LDAXC-SIC) potential of the fullerene. In the range of impact energies covered in the present work, the collision velocities are always smaller than the velocity of one electron in any orbital. This fact justifies the use of the quasimolecular approach for the description of the ion-atom (ion-cluster) collision. For further details see Refs. [64,65].

We have calculated charge transfer cross sections for the present $C^{6+} + C_{60}$ collisions within the inclusive probability method [63]. This method has been successfully used earlier to treat charge transfer collisions between metal clusters and atoms or ions [64–67]. We first calculate the total probability $P_{\rm CT}(b,q)$ for removing exactly q electrons from the fullerene (by means of charge transfer to the C^{6+} ion) as a function of the impact parameter b. The corresponding charge transfer cross section is

$$\sigma_{\rm CT}(q) = 2\pi \int_{R_C}^{\infty} b P_{\rm CT}(b,q) db, \tag{1}$$

where $R_C = 6.7$ a$_0$ is the fullerene radius. We use impact parameters from $b = R_C$ due to the jellium description of C_{60}. This procedure was repeated for $q = 1$–6, i.e., for removal of one to six electrons from C_{60} producing C_{60}^{+} through C_{60}^{6+}.

Figure 2 shows the correlation diagram for the relevant molecular orbitals of $(C_{60} + C)^{6+}$. Three main regions contribute to the charge transfer processes: $R \sim 20$ a.u. capture from inner molecular orbitals to $n = 5$, $R \sim 30$ a.u. capture from $2g$ and $2h$ to $n = 6$, and $R \sim 40$ a.u. capture from $2h$ to $n = 7$.

B. Fullerene excitation energy

Electron capture can take place from inner orbitals of the fullerene, thus leading to an electronically excited charged cluster. We define the electronic energy deposited in the fullerene after the charge transfer for each produced C_{60}^{q+} at given impact parameter and collision energy as

$$E_{\rm dep}^{q+}(b) = \sum_{s}^{N_s} P^s(b)\left(E_{\rm excited}^{s,q+} - E_{\rm ground}^{q+}\right). \tag{2}$$

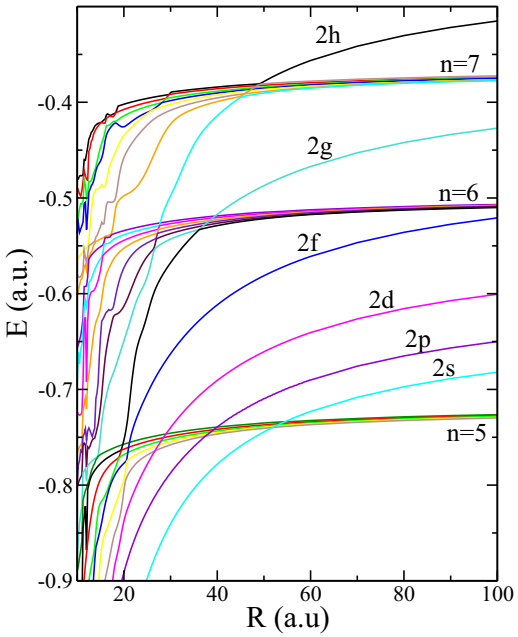

FIG. 2. (Color online) Correlation diagram for the relevant molecular orbitals of $(C_{60} + C)^{6+}$ denoted by their character at infinite separation: $n = 5$, 6, and 7 orbitals from C^{6+} and π $2s$, $2p$, $2d$, $2f$, $2g$, and $2h$ orbitals from C_{60}.

The sum runs over all possible N_s electronic states created after the charge transfer of q electrons ($N_s = 12, 66, 220, 495, 792$, and 924 for $q = 1, 2, 3, 4, 5$, and 6, respectively, within the spherical electronic structure used for the description of the fullerene). The excitation probability for each state $P^s(b)$ has been previously computed using the inclusive probability method [63]. $E_{\rm excited}^{s,q+}$ is the electronic energy of the created state s just after the collision (before relaxation) and is given by

$$E_{\rm excited}^{s,q+} = \sum_i \epsilon_i, \tag{3}$$

with ϵ_i being the energy of the occupied KS orbitals after the collision. $E_{\rm ground}^{q+}$ is the electronic energy of the C_{60}^{q+} molecule when it is electronically relaxed

$$E_{\rm ground}^{q+} = \sum_i \epsilon_i', \tag{4}$$

where $\epsilon_i' = \epsilon_i - q/R_C$, the energies of the Kohn-Sham orbitals for a q times charged fullerene (ϵ_i are the orbital energies for the neutral systems) [68].

The total excitation energy E_{60}^{*} is given by the electronic energy deposited due to nonvalence electron capture and due to the temperature T of the fullerene before the collision

$$E_{60}^{*} = E_{\rm dep}^{q+} + E_T. \tag{5}$$

We computed the internal energy due to temperature with the Dulong-Petit formula for an ensemble of harmonic oscillators

$$E_T = (3N_{\rm at} - 6)k_B T. \tag{6}$$

$N_{\rm at}$ is the number of atoms in the fullerene and k_B is the Boltzmann constant.

C. Statistical fragmentation

The excited charged fullerenes can transfer their electronic excitation energy to the internal modes through electron-phonon coupling, leading to vibrational excitations and possibly also fragmentation. In this work we use a statistical fragmentation model based on the Weisskopf theory [69]. It is a first-order time-dependent perturbation (and statistical) approach, initially proposed to study the decay phenomena in nuclear physics and successfully employed for the treatment of metal clusters [65–67,70] and small carbon clusters [71,72]. Using this method we obtain an analytical form for the evaluation of the fragmentation rate constants, which reduces the computational cost with respect to molecular dynamics simulation. In the case of neutral C_2 evaporation the formalism has already been presented in Ref. [65]. Here, we extend this formalism for the description of the C_2^+ fission.

Given a quantum system described by the Hamiltonian $H = H_0(t_i = 0) + H'(t > 0)$, in which H_0 represents the nonperturbed system at $t = 0$ and H' is a constant perturbation for $t > 0$, the number of transitions due to the perturbation $N_{i\to f}$ from an initial state ψ_i to a closely related set of final states $\{\psi_f\}$ is given by

$$\frac{dN_{i\to f}}{dt} = \frac{2\pi}{\hbar}|H'_{i\to f}|^2\rho_f, \tag{7}$$

where $H'_{i\to f} = \int_{-\infty}^{+\infty}\psi_f^*(r)H'\psi_i(r)d^3r$, is the matrix element for a transition between the initial and final states $\psi_i \to \psi_f$. The final state density is ρ_f. Equation (7) is Fermi's golden rule and gives the transition rate $k \equiv \frac{dN_{i\to f}}{dt}$, from one initial state ψ_i to a set of possible final states around ψ_f.

Here, we evaluate the fragmentation of an exited charged fullerene by assuming sequential mechanisms where C_2 evaporation is in competition with C_2^+ fission (see Fig. 3)

$$C_{58}^{q+} + C_2 \underset{k_{60,2}^{\rm evap}}{\longleftarrow} \left(C_{60}^{q+}\right)^* \underset{k_{60,2}^{\rm fiss}}{\longrightarrow} C_{58}^{(q-1)+} + C_2^+ \tag{8}$$

For the loss of a neutral C_2 molecule [left-hand side of Eq. (8)], the rate constant depends on the excitation energy, $k_{60,2}^{\rm evap}(E_{60}^*)$. The ejected C_2 may carry some kinetic (e) and vibrational (x) energy with it. Then, if the energy required to remove a neutral C_2 from C_{60}^{q+} is $D_{60,2}$, the resulting C_{58}^{q+} fullerene will have an internal excitation energy

$$E_{58}^* = E_{60}^* - D_{60,2} - x - e. \tag{9}$$

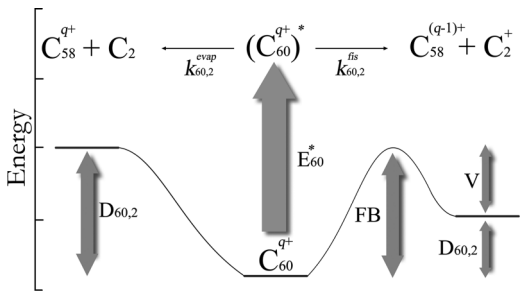

FIG. 3. Schematic energy profile for the excitation, C_2 evaporation, and C_2^+ asymmetric fission. Dissociation energies, fission barriers, and rate constants are shown.

Thus, in $(C_{60}^{q+})^* \to C_{58}^{q+} + C_2$ reactions (C_2 evaporation), the density of final states is

$$\rho_f = \int dx \int_0^{E_{60}^* - D_{60,2} - x} \rho_{58}(E_{58}^*)\rho_2(x,e)de, \tag{10}$$

where $\rho_{58}(E_{58}^*) = \rho_{58}(E_{60}^* - D_{60,2} - x - e)$ and $\rho_2(x,e)$ are the densities of states of C_{58}^{q+} and C_2, respectively. The latter is associated with two degrees of freedom, the vibration ($\rho_{v,2}$) of the C–C bond and the translation ($\rho_{t,2}$) of the molecule, and can be separated as well: $\rho_2(x,e) = \rho_{v,2}(x)\rho_{t,2}(e)$. The translational density of states of C_2 is

$$\rho_{t,2}(e) = \int \frac{p}{(2\pi\hbar)^3}\delta\left(e - \frac{p^2}{2m_2}\right)d^3r\,d^3p = \frac{\Omega 4\pi m_2 p}{(2\pi\hbar)^3}, \tag{11}$$

where $\frac{p^2}{2m_2}$ is the C_2 kinetic energy. The vibrational density of states $\rho_{v,2}(x)$ is

$$\rho_{v,2}(x) = \frac{1}{\hbar w_d}\Theta(D_{2,1} - x), \tag{12}$$

where Θ is the Heaviside function and $x \in [0, D_{2,1}]$, being $D_{2,1}$ the dissociation energy of C_2, and w_d the vibrational frequency. It has been shown by the authors of Ref. [73] that the rotational energies are much smaller than the vibrational energies for C_2 emitted from charged fullerenes and the former are thus not included in the present discussion.

To evaluate $H'_{i\to f}$, we consider the reverse reaction (molecular fusion) with the rate

$$\frac{dN_{f\to i}}{dt} = \frac{2\pi}{\hbar}|H'_{f\to i}|^2\rho_i = j\sigma(e). \tag{13}$$

The flux j is

$$j = \frac{p}{m_2\Omega}, \tag{14}$$

where p is the momentum, m_2 is the reduced mass of the ejected dimer, and Ω is the normalization volume. Using the principle of detailed balance [74]

$$|H'_{f\to i}|^2 = |H'_{i\to f}|^2 \tag{15}$$

and taking into account that $\rho_i = \rho_{60}(E_{60}^*)$, we have

$$|H'_{i\to f}|^2 = \frac{\hbar}{2\pi}\frac{j\sigma(e)}{\rho_{60}(E_{60}^*)} = \frac{\hbar}{2\pi}\frac{p}{m_2\Omega}\frac{\sigma(e)}{\rho_{60}(E_{60}^*)}. \tag{16}$$

Using $e = \frac{p^2}{2m_2}$ and Eqs. (10)–(12) and (16), the C_2 emission rate [Eq. (7)] can now be rewritten as

$$k_{60,2}^{\rm evap} = \frac{m_2}{\pi^2\hbar^4 w_d}\int_0^{\alpha} dx \int_0^{E_{60}^* - D_{60,2} - x} \frac{\rho_{58}(E_{58}^*)}{\rho_{60}(E_{60}^*)}\sigma(e)ede \tag{17}$$

with

$$\alpha = \begin{cases} E_{60}^* - D_{60,2} & \text{if} \quad E_{60}^* - D_{60,2} \leqslant D_{2,1}, \\ D_{2,1} & \text{if} \quad E_{60}^* - D_{60,2} > D_{2,1}, \end{cases}$$

with E_{58}^* given by Eq. (9). For the loss of C_2^+ [right-hand side of Eq. (8)], two charged species interact after the fragmentation giving a Coulomb potential barrier as shown schematically in Fig. 3. The total energy (internal plus translational) of the $C_{58}^{(q-1)+} + C_2^+$ system is between $V = V_{FB} - D_{60,2^+}$ and

$E^*_{60} - D_{60,2^+} - x - e$, where V_{FB} is the fission barrier, $D_{60,2^+}$ is the dissociation energy (i.e., the energy difference between the initial C_{60}^{q+} and the final $C_{58}^{(q-1)+} + C_2^+$ ground-state energies), and V is the molecular fusion barrier. The vibrational energy of C_2^+ is x and its kinetic energy is e. Thus, we have for the fission a rate constant

$$k^{\rm fiss}_{60,2} = \frac{m_2}{\pi^2\hbar^4 w_d}\int_0^{\alpha} dx \int_V^{E^*_{60}-D_{60,2}-x} \frac{\rho_{58}(E^*_{58})}{\rho_{60}(E^*_{60})}\sigma(e)ede \tag{18}$$

with

$$\alpha = \begin{cases} E^*_{60} - D_{60,2} - V & \text{if} \quad E^*_{60} - D_{60,2} - V \leqslant D_{2,1}, \\ D_{2,1} & \text{if} \quad E^*_{60} - D_{60,2} - V > D_{2,1}. \end{cases}$$

The density of states of the parent C_{60}^{q+} and produced ($C_{58}^{q+}C_{58}^{(q-1)+}$) clusters are given by a combination of the different contributions: translational, vibrational, and rotational. We can neglect the translation of these clusters because the ejected dimer carry most of the translational energy. We further use the approximation $\frac{\rho_{r,58}}{\rho_{r,60}} \approx 1$, i.e., we are assuming that the densities of rotational states ρ_r are the same for C_{60} and C_{58}. We take the fullerene vibrational density of states in the harmonic approximation

$$\rho_v(E^*) = \frac{(E^*)^{(g-1)}}{\Gamma(g)\prod_{j=1}^{g}(h\upsilon_j)}, \tag{19}$$

where g is the number of vibrational degrees of freedom, υ_j is the frequency of its jth vibrational mode, and Γ is the Euler's gamma function.

Furthermore, in the original Weisskopf formulation [69], the cross section is defined as

$$\sigma(e > V) = \pi R_C^2\left(1 - \frac{V}{e}\right), \tag{20}$$

where V is a Coulomb barrier (see Fig. 3) and R_C is the cluster radius. When the two charged fragments approach each other, $C_{58}^{(q-1)+} + C_2^+ \rightarrow C_{60}^{q+}$, a Coulomb potential barrier appears $V \neq 0$ and the geometrical cross section is weighted by the relation between the kinetic energy of the dimer and the barrier. In the case of neutral C_2 evaporation $V = 0$ and thus the cross section is just the geometrical one $\sigma = \pi R_C^2$. With these considerations, Eqs. (17)–(19) and (20) give

$$k^{\rm evap}_{60,2} = \phi \begin{cases} (E^*_{60} - D_{60,2})^{(g+2)} & \text{if} \quad E^*_{60} - D_{60,2} \leqslant D_{2,1}, \\ (E^*_{60} - D_{60,2})^{(g+2)} - (E^*_{60} - D_{60,2} - D_{2,1})^{(g+2)} & \text{if} \quad E^*_{60} - D_{60,2} > D_{2,1}, \end{cases} \tag{21}$$

and

$$k^{\rm fiss}_{60,2} = \phi \begin{cases} (E^*_{60} - D_{60,2} - V)^{(g+2)} & \text{if} \quad E^*_{60} - D_{60,2} - V \leqslant D_{2,1}, \\ (E^*_{60} - D_{60,2} - V)^{(g+2)} - (E^*_{60} - D_{60,2} - D_{2,1} - V)^{(g+2)} & \text{if} \quad E^*_{60} - D_{60,2} - V > D_{2,1}, \end{cases} \tag{22}$$

with

$$\phi = \frac{\pi R_C^2}{(E^*_{60})^{(f-1)}}\frac{1}{g}\frac{1}{(g+1)}\frac{1}{(g+2)}\frac{m_2}{\pi^2\hbar^4 w_d}\frac{\Gamma(f)\prod_{i=1}^{f}(h\upsilon_i)}{\Gamma(g)\prod_{j=1}^{g}(h\upsilon_j)}.$$

The input data needed to evaluate the rate constants are dissociation energies, fission barriers, and vibrational frequencies. They have been taken from density functional theory calculations [50,51].

In this work we are interested in evaluating the competition between evaporation and fission as a function of the charge, excitation energy, and time after the excitation. We thus consider the first step in the fragmentation of $(C_{60}^{q+})^*$ assuming the scheme in Eq. (8). After the evaluation of the fragmentation rate constants, a set of coupled equations is integrated in time to obtain the probability of no fragmentation $P_{C_{60}^{q+}}$, evaporation $P_{C_{58}^{q+}}$, and fission $P_{C_{58}^{(q-1)+}}$ at a given excitation energy. We integrate in time the equations until $t = t_{\rm max}$; $t_{\rm max}$ is the experimental time window for measuring the decay, which depends on the type of mass spectrometer (but is of the same order of magnitude as the time of flight)

$$\begin{aligned} P_{C_{60}^{q+}} &= \exp\left[-\left(k^{\rm evap}_{60,2} + k^{\rm fiss}_{60,2}\right)t_{\rm max}\right], \\ P_{C_{58}^{q+}} &= \frac{k^{\rm evap}_{60,2}}{\left(k^{\rm evap}_{60,2} + k^{\rm fiss}_{60,2}\right)}\left(1 - P_{C_{60}^{q+}}\right), \\ P_{C_{58}^{(q-1)+}} &= \frac{k^{\rm fiss}_{60,2}}{\left(k^{\rm evap}_{60,2} + k^{\rm fiss}_{60,2}\right)}\left(1 - P_{C_{60}^{q+}}\right), \end{aligned} \tag{23}$$

where the probabilities, $P_{C_{60}^{q+}}$, $P_{C_{58}^{q+}}$, and $P_{C_{58}^{(q-1)+}}$ depend on $k^{\rm evap}_{60,2}[E^*_{60}(b)]$ and $k^{\rm fiss}_{60,2}[E^*_{60}(b)]$. We allow C_2 emission to take place if $E > D_{60,2}$ and C_2^+ emission if $E > V_{FB}$, i.e., we open the fragmentation channels only if they are energetically accessible.

Finally, we combine the charge transfer with the fragmentation probabilities to obtain the cross sections for the production of C_{60}^{q+}, C_{58}^{q+}, and $C_{58}^{(q-1)+}$:

$$\begin{aligned} \sigma_{C_{60}^{q+}} &= 2\pi\int_{R_C}^{\infty} b[P_{\rm CT}(b)]\left[P_{C_{60}^{q+}}\right]db, \\ \sigma_{C_{58}^{q+}} &= 2\pi\int_{R_C}^{\infty} b[P_{\rm CT}(b)]\left[P_{C_{58}^{q+}}\right]db, \\ \sigma_{C_{58}^{(q-1)+}} &= 2\pi\int_{R_C}^{\infty} b[P_{\rm CT}(b)]\left[P_{C_{58}^{(q-1)+}}\right]db. \end{aligned} \tag{24}$$

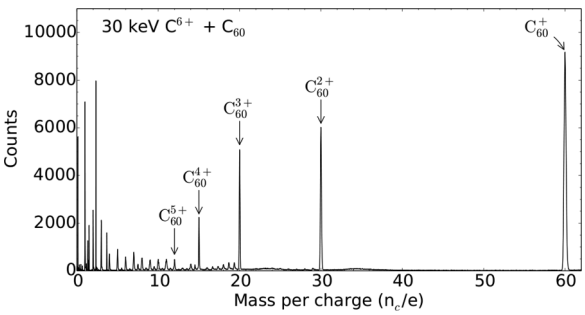

FIG. 4. Mass spectrum due to 30 keV $C^{6+} + C_{60}$ collisions.

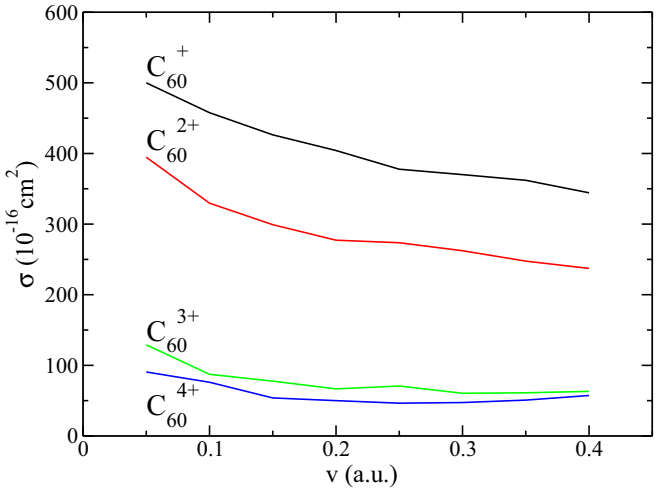

FIG. 5. (Color online) Computed absolute charge transfer cross sections (in 10^{-16} cm^2) in $C_{60} + C^{6+}$ collisions as a function of the impact velocity (in a.u.).

IV. RESULTS AND DISCUSSION

In Fig. 4 we show a typical mass spectrum recorded in 30 keV C^{6+} + C_{60} collisions. The intensity distribution is similar to those at higher collision energies (not shown) and is dominated by intact C_{60}^{q+} ions (q = 1–5), but large fragments such as C_{58}^{q+} are also present for $q > 2$. These high-mass peaks stem from distant electron transfer collisions where little energy is deposited in nuclear and electronic stopping processes, while the low-mass peaks are due to Coulomb explosions of highly charged and highly excited C_{60}^{q+} ions formed at smaller impact parameters.

The calculated cross sections for the production of C_{60}^{q+} ions, $\sigma_{C_{60}^{q+}}$, are shown in Fig. 5. In all cases σ decreases with the collision velocity. σ decreases also with the charge state, being much smaller for $q = 3$ and 4. The cross sections

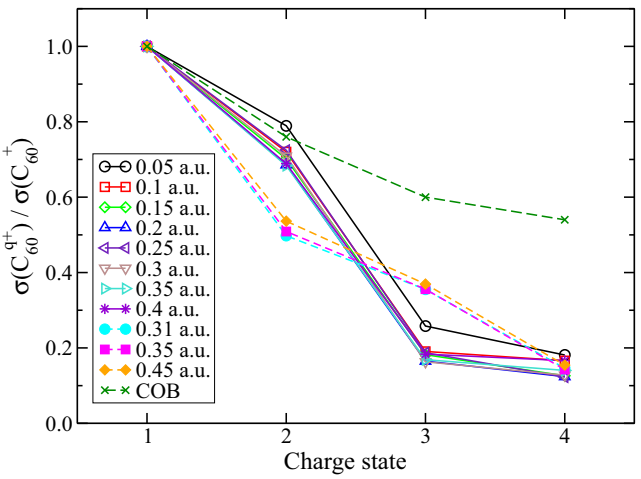

FIG. 6. (Color online) Relative charge transfer cross sections $\sigma(C_{60}^{q+})/\sigma(C_{60}^{+})$ as a function of the charge state. Open symbols full lines: theoretical simulations, filled symbols dashed lines: experiments, "X"-dashed line: classical over-the-barrier (COB) model. Lines between the data points are to guide the eye.

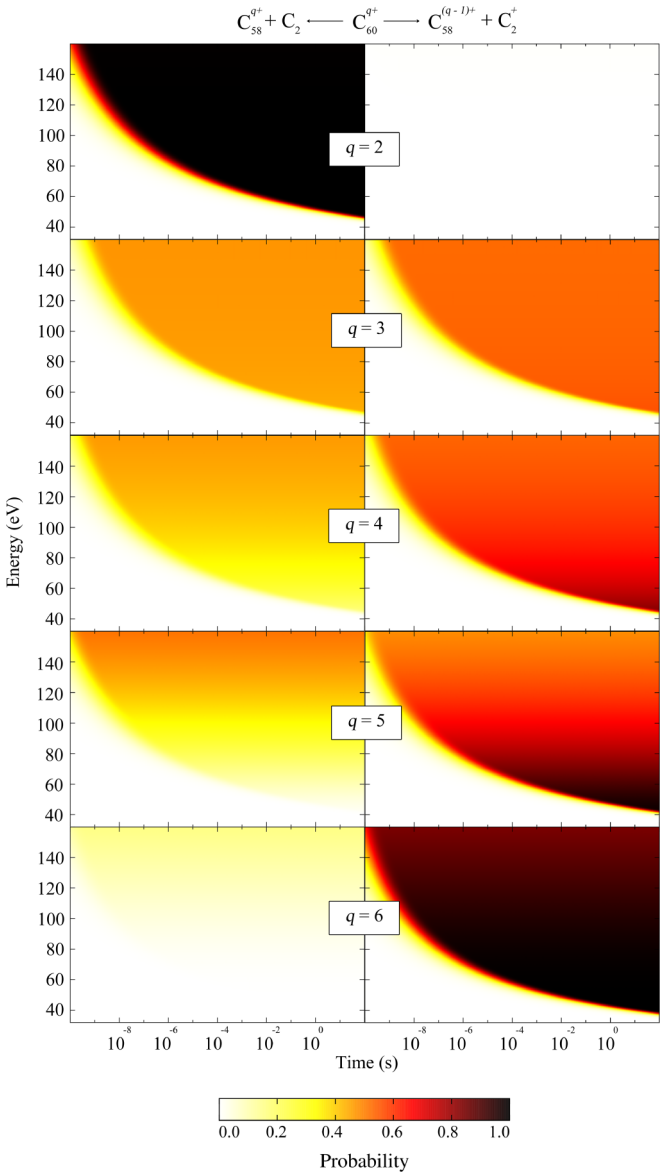

FIG. 7. (Color online) C_2 evaporation (left column) and C_2^+ asymmetric fission (right column) probabilities as functions of the excitation energy and the time after excitation.

in Fig. 5 are higher than the ones obtained within a simple classical over-the-barrier model, showing that capture at large distances plays an important role (see the correlation diagram in Fig. 2). A comparison between the experimental and theoretical relative cross sections $\sigma(C_{60}^{q+})/\sigma(C_{60}^{+})$ is given in Fig. 6. The trend is qualitatively reproduced by the simulations, being slightly overestimated for $q = 2$, underestimated for $q = 3$, and correctly predicted for $q = 4$.

Figure 7 presents the fragmentation behavior obtained in our simulations: probabilities of fission and evaporation are shown as a function of the time after excitation, and of the fullerene internal energy $E = E_{60}^{*} + E_T$ ($T = 800$ K). For the neutral, singly, and doubly charged C_{60} no fission is observed, as expected (see upper right panel of the figure). For these charge states evaporation is the dominant fragmentation channel in the whole range of excitation energy and time. For

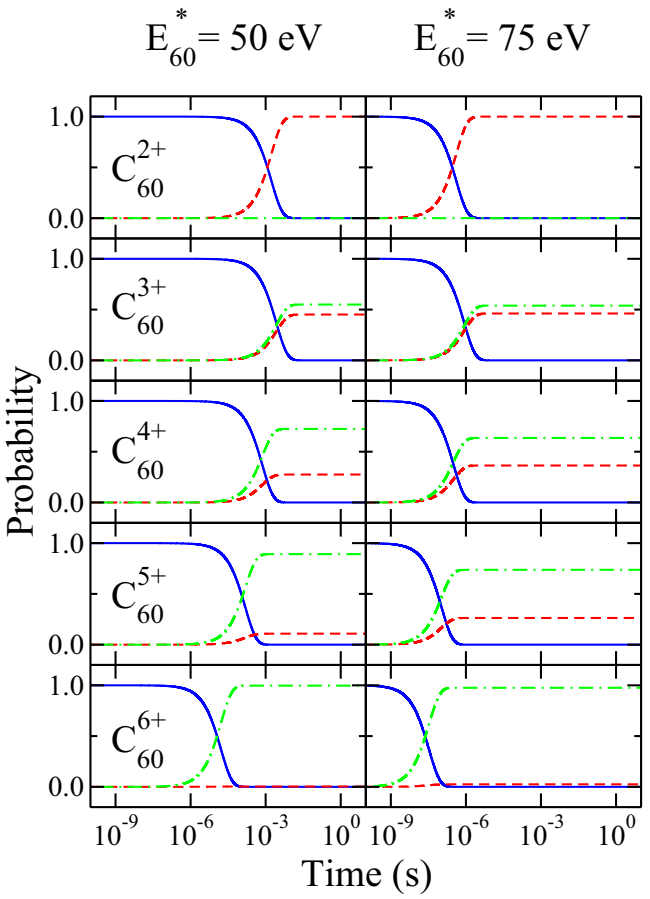

FIG. 8. (Color online) C_2 evaporation and C_2^+ asymmetric fission probabilities as a function of the time of flight at given two typical values of excitation energy. Internal excitation energy due to the temperature E^*_{Temp}, included for $T = 800$ K. Solid blue, dashed red, and dotted-dashed green lines represent C_{60}^{q+}, C_{58}^{q+}, and $C_{58}^{(q-1)+}$, respectively.

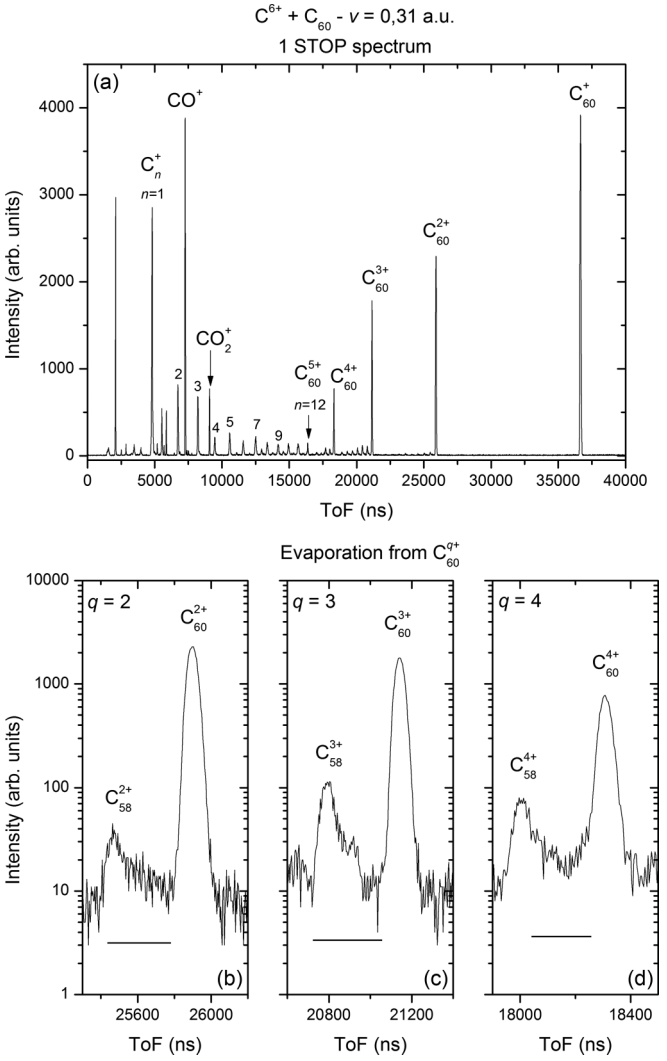

FIG. 9. Time-of-flight distribution of the cationic products in the 1-STOP spectrum (only one charged fragment detected) after collisions of C^{6+} and C_{60} at $v = 0.31$ a.u.. Zoom-ins of regions around C_{60}^{2+}, C_{60}^{3+}, and C_{60}^{4+} are shown in panels (b), (c), and (d), respectively. Horizontal lines in lower panels show the typical tail corresponding to delayed fragmentation during extraction time.

$q = 3$, 4, and 5 we observe competition between fission and evaporation in certain regions of time and energy. For $q = 6$ fission dominates, and almost no evaporation is observed (see lower left panels of the figure).

Figure 8 shows fission and evaporation probabilities as a function of the time after excitation computed for two values of excitation energy $E_{C_{60}^*} = 50$ and 75 eV. The typical experimental value of extraction time after excitation is $\sim 10^{-6}$ s, and thus, the figure give us a hint for the interpretation of the experiments, in particular competition between evaporation and fission in the first step of the fragmentation: $C_{58}^{(q-1)+} \leftarrow (C_{60}^{q+})^* \rightarrow C_{58}^{q+}$. At low excitation energies (50 eV) C_{60}^{2+} does not start fragmentation until a time about 10^{-3} s is reached, i.e., in these conditions, after the collision process has taken place a metastable $(C_{60}^{2+})^*$ remains intact for $\sim 10^{-3}$ s, even when the excitation energy is five times larger than the energy required for C_2 evaporation [41]. However, when the excitation energy increases to 75 eV, the time to observe fragmentation decreases: it takes place at the experimental extraction time $t \sim 10^{-6}$ s. For a larger excitation energy ($E = 100$ eV, not shown in the figure) the fragmentation is over before the extraction time in the experiment. When the charge increases, the fragmentation is faster and appears at shorter time. For C_{60}^{6+} at 50 eV, the C_{58}^{5+} probability, which comes from the fission channel and is the dominant process, is about 2.5% at $t = 10^{-6}$ s; and reaches 99.5% at $t = 5.45 \times 10^{-3}$ s. In the 75-eV case, from $q = 3$ to $q = 5$, both C_2 and C_2^+ emission processes occur on time scales corresponding to that for extraction in the experiment.

A comparison between the simulations and the experimental measurements has been carried out by analyzing the so-called 1-STOP spectrum (Fig. 9). It shows fragments which are produced without any other cationic species in the same event. Smaller fullerenes, such as C_{58}^{q+} due to emission of neutral C_2 molecules, are also recorded. A detailed analysis of the shapes of the peaks observed in this spectrum (see the zoom-in in Fig. 9) shows the typical "tail" corresponding to delayed fragmentation during the extraction time of a few microseconds. These observations agree with our simulations

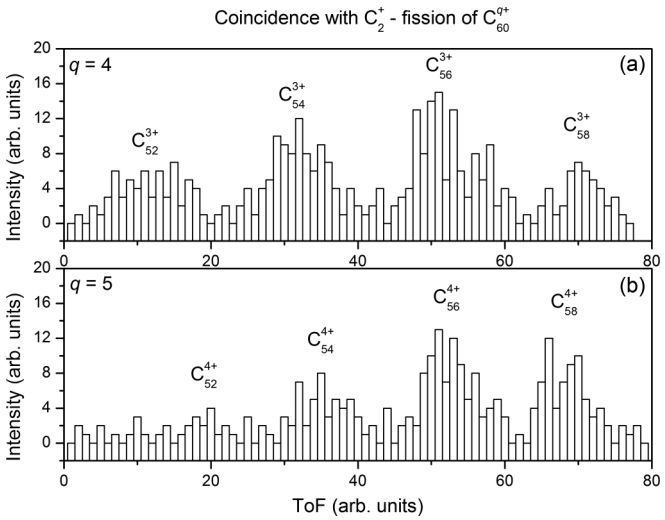

FIG. 10. Time-of-flight of $C_n^{(q-1)+}$ ions measured in coincidence with C_2^+ in $C^{6+} + C_{60}$ collisions at $v = 0.45$ a.u.

with excitation energies of ∼75 eV and fragmentation times of $t \sim 10\ \mu$s (see Fig. 8).

In Fig. 10 we show the spectra for C_n^{q+} fullerenes detected in coincidence with C_2^+. The fission is not observed for charge states lower than four. Our calculations show a similar behavior: In Fig. 11 we show the fragmentation cross sections evaluated within the Weisskopf formalism. For this, evaporation and fission rate constants have been computed employing the deposited energy as a function of the impact parameter. These results are for $v_{col} = 0.05 - 0.3$ a.u., and charges $q = 2 - 6$, and are shown for different detection times. The cross sections are higher for the lower velocities, which can be understood since the target excitation processes become more effective in these cases. In agreement with the assumption of a more efficient excitation leading to fragmentation at low impact velocities. As expected, the fragmentation cross section of evaporation and fission are comparable for intermediate charge states, being evaporation dominant for $q = 2$ and fission for $q = 6$.

Our fragmentation simulations are also in good agreement with other recent experimental measurements. Reinkoster *et al.* [75] who reported ionization and fragmentation of C_{60} after excitation by synchrotron radiation in the energy range 26–130 eV. Fragmentation of C_{60}^+ and C_{60}^{2+} was not observed at $t = 8\ \mu$s for an excitation energy of 41 eV by Reinkoster *et al.* [75]. Our Weisskopf calculations show that fragmentation starts at ∼ 50 eV, showing that intact C_{60}^+ and C_{60}^{2+} species will be detected at lower values of excitation energy, also in agreement with the authors of Refs. [76,77]. In Ref. [75] C_{58}^+ production was observed at 65 eV of excitation energy (in agreement with our results). At higher excitation energy the small observed yield of C_{58}^+ is due to further C_2 evaporation From C_{58}^+ [78].

Concerning ion-fullerene collisions, recent experiments [22,23] have measured the internal energy of fragmented doubly and triply charged fullerenes prepared in collisions $H^+ + C_{60} \rightarrow H^- + (C_{60}^{2+})^*$, and $F^{2+} + C_{60} \rightarrow F^- + (C_{60}^{3+})^*$, respectively. A wide distribution of excitation energies is measured in the emission of C_2 from C_{60}^{2+} (within an extraction time of 3.5 μs). Evaporation from the triply charged fullerene, $C_{60}^{3+} \rightarrow C_{58}^{3+} + C_2$, was observed with an excitation energy distribution centered on ∼50 eV. In these experiments, thermal electronic ionization of $(C_{60}^{3+})^*$ leads to C_{60}^{4+} which may decay further via dissociation. The energy distribution estimations are also in good agreement with our simulations (see also Ref. [78]). The measured excitation energy distributions in the fragmentation of C_{60}^{4+} are in the energy range 40–100 eV centered at ∼60 eV both for C_2 and C_2^+ emission on the experimental time scale [79]. Intact fullerene ions were observed for excitation energies of about 30 eV while about 80 eV was required for observation of C_{58}^{2+} and C_{58}^{3+} on the

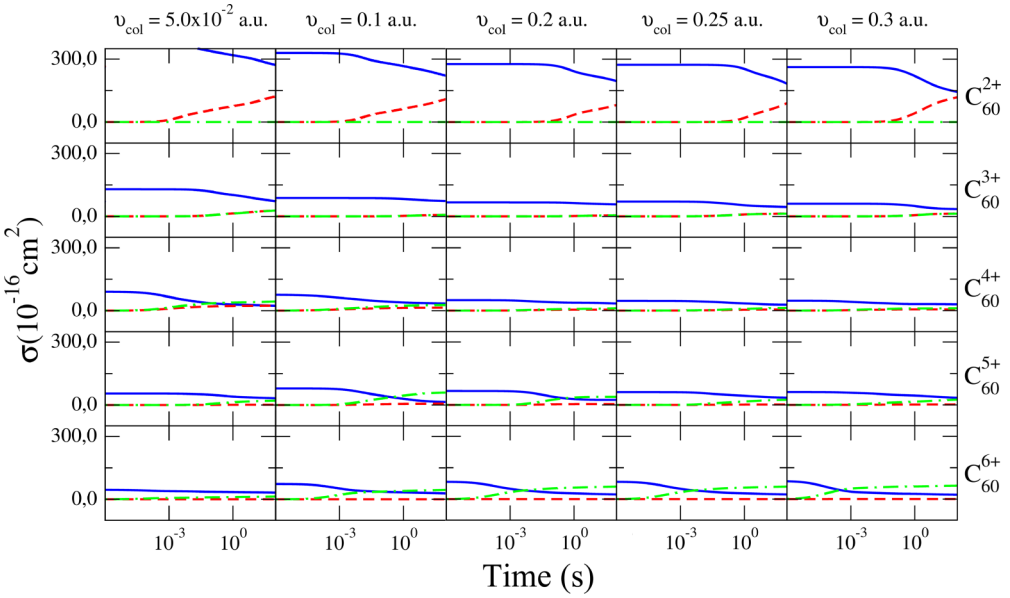

FIG. 11. (Color online) Calculated cross sections for producing intact C_{60}^{q+} ions (solid blue curve), and C_{58}^{q+} and $C_{58}^{(q-1)+}$ fragments (dashed red and dashed-dotted green curves, respectively) as functions of time for $C^{6+} + C_{60}$ collisions at five different velocities (see text).

experimental time scale in Ref. [79], which is consistent with our simulations. In the case of highly charged fullerenes, collisions of 280 keV Xe^{25+} on C_{60} allowed to measure an average lifetime of 1.1 μs where the decay was dominated by $C_{60}^{6+} \rightarrow C_{58}^{5+} + C_2^+$ [80]. If we assume an excitation energy of ~60–80 eV this lifetime is in agreement with our calculations.

V. CONCLUSION

We have presented a combined experimental and theoretical study on charge-transfer, excitation and fragmentation in $C^{6+} + C_{60}$ collisions. From the theoretical point of view we present a computational strategy that allows a quantitative description of the main ionization and fragmentation processes without any fitting parameters. We have treated Coulomb fission barriers for the emission of C_2^+ ions from C_{60}^{q+} within the Weisskopf formalism to achieve this goal. From the experimental point of view the detection in coincidence of charged fragments allows to distinguish different channels.

We have shown that charge transfer cross sections decrease with the number of electrons being transferred from the fullerene and with the impact velocity. The highly charged fullerenes produced in the collision mainly get rid of part of their excess energy through bond cleavage. In particular, we have observed strong competition between C_2 and C_2^+ emission for C_{60} charge states $q = 3$, 4, and 5 in the time-of-flight range studied. For low charge states ($q < 2$) evaporation of neutral C_2 dominates while C_2^+ emission dominates for high charge states ($q = 6$). Fragmentation measured in the typical experimental time scales (μs) correspond to energy deposits in the collision of the order of a few tens of electronvolts (~50–100 eV). Our theoretical predictions are consistent with the present measurements and with other recent experimental studies.

ACKNOWLEDGMENTS

We acknowledge the generous allocation of computer time at the Centro de Computación Científica at the Universidad Autónoma de Madrid (CCC-UAM). This work was partially supported by the Spanish Ministry of Science and Innovation (MICINN) Projects No. FIS2010-15127, No. CTQ2010-17006, and No. CSD2007-00010 and Comunidad de Madrid (CAM) Project No. S2009/MAT1726. H.S. Jr., gratefully acknowledges the support of the Erasmus Mundus programme of the European Union (FPA 2010-0147). S.D.-T. gratefully acknowledges the "Ramón y Cajal" program of the Spanish Ministerio de Educación y Ciencia and the Université de Caen Basse-Normandie for a visiting professor support. This work was also supported by the Swedish Research Council (Contracts No. 621-2012-3662, No. 621-2012-3660, and No. 621-2011-4047). We acknowledge the COST action CM1204 "XUV/X-ray light and fast ions for ultrafast chemistry (XLIC)." The experimental studies have been performed at the ARIBE facility, the low-energy ion beam facility of GANIL (Caen, France). Financial support received from the CNRS PICS-05356 program, the ANR Programme Blanc PIBALE/ANR-09-BLAN-013001, and the Conseil Régional de Basse-Normandie is gratefully acknowledged. This research was conducted in the scope of the International Associated Laboratory (LIA) "Fragmentation Dynamics of complex Molecular systems (DYNAMO)."

[1] J. de Vries, H. Steger, B. Kamke, C. Menzel, B. Weisser, W. Kamke, and I. V. Hertel, Chem. Phys. Lett. **188**, 159 (1992).

[2] S. W. J. Scully, E. D. Emmons, M. F. Gharaibeh, R. A. Phaneuf, A. L. D. Kilcoyne, A. S. Schlachter, S. Schippers, A. Müller, H. S. Chakraborty, M. E. Madjet, and J. M. Rost, Phys. Rev. Lett. **94**, 065503 (2005).

[3] A. Rüdel, R. Hentges, U. Becker, H. S. Chakraborty, M. E. Madjet, and J. M. Rost, Phys. Rev. Lett. **89**, 125503 (2002).

[4] D. Hathiramani, K. Aichele, W. Arnold, K. Huber, E. Salzborn, and P. Scheier, Phys. Rev. Lett. **85**, 3604 (2000).

[5] S. Matt, O. Echt, R. Wörgötter, P. Scheier, C. E. Klots, and T. D. Märk, Int. J. Mass Spectrom. **167**, 753 (1997).

[6] A. Itoh, H. Tsuchida, K. Miyabe, T. Majima, and N. Imanishi, J. Phys. B: At. Mol. Opt. **32**, 277 (1999).

[7] P. Scheier, B. Dunser, R. Wörgötter, D. Muigg, S. Matt, O. Echt, M. Foltin, and T. D. Märk, Phys. Rev. Lett. **77**, 2654 (1996).

[8] M. O. Larsson, P. Hvelplund, M. C. Larsen, H. Shen, H. Cederquist, and H. T. Schmidt, Int. J. Mass Spectrom. **177**, 51 (1998).

[9] T. LeBrun, H. G. Berry, S. Cheng, R. W. Dunford, H. Esbensen, D. S. Gemmell, E. P. Kanter, and W. Bauer, Phys. Rev. Lett. **72**, 3965 (1994).

[10] T. Schlatholter, O. Hadjar, R. Hoekstra, and R. Morgenstern, Phys. Rev. Lett. **82**, 73 (1999).

[11] H. Cederquist, A. Fardi, K. Haghighat, A. Langereis, H. T. Schmidt, S. H. Schwartz, J. C. Levin, I. A. Sellin, H. Lebius, B. Huber, M. O. Larsson, and P. Hvelplund, Phys. Rev. A **61**, 022712 (2000).

[12] J. Opitz, H. Lebius, S. Tomita, B. A. Huber, P. Moretto Capelle, D. Bordenave-Montesquieu, A. Bordenave-Montesquieu, A. Reinkoster, U. Werner, H. O. Lutz, A. Niehaus, M. Benndorf, K. Haghighat, H. T. Schmidt, and H. Cederquist, Phys. Rev. A **62**, 022705 (2000).

[13] S. H. Schwartz, A. Fardi, K. Haghighat, A. Langereis, H. T. Schmidt, and H. Cederquist, Phys. Rev. A **63**, 013201 (2000).

[14] O. Hadjar, P. Foldi, R. Hoekstra, R. Morgenstern, and T. Schlatholter, Phys. Rev. Lett. **84**, 4076 (2000).

[15] S. Martin, L. Chen, A. Denis, R. Bredy, J. Bernard, and J. Desesquelles, Phys. Rev. A **62**, 022707 (2000).

[16] P. Moretto-Capelle, D. Bordenave-Montesquieu, A. Rentenier, and A. Bordenave-Montesquieu, J. Phys. B: At. Mol. Opt. **34**, L611 (2001).

[17] M. J. Jamieson and B. Zygelman, Phys. Rev. A **64**, 032703 (2001).

[18] S. Tomita, H. Lebius, A. Brenac, F. Chandezon, and B. A. Huber, Phys. Rev. A **65**, 053201 (2002).

[19] A. Rentenier, D. Bordenave-Montesquieu, P. Moretto-Capelle, and A. Bordenave-Montesquieu, J. Phys. B: At. Mol. Opt. **36**, 1585 (2003).

[20] S. Tomita, H. Lebius, A. Brenac, F. Chandezon, and B. A. Huber, Phys. Rev. A **67**, 063204 (2003).

[21] J. Jensen, H. Zettergren, H. T. Schmidt, H. Cederquist, S. Tomita, S. B. Nielsen, J. Rangama, P. Hvelplund, B. Manil, and B. A. Huber, Phys. Rev. A **69**, 053203 (2004).

[22] L. Chen, S. Martin, J. Bernard, and R. Brédy, Phys. Rev. Lett. **98**, 193401 (2007).

[23] S. Martin, L. Chen, A. Salmoun, B. Li, J. Bernard, and R. Brédy, Phys. Rev. A **77**, 043201 (2008).

[24] A. Rentenier, L. F. Ruiz, S. Díaz-Tendero, B. Zarour, P. Moretto-Capelle, D. Bordenave-Montesquieu, A. Bordenave-Montesquieu, P.-A. Hervieux, M. Alcamí, M. F. Politis, J. Hanssen, and F. Martín, Phys. Rev. Lett. **100**, 183401 (2008).

[25] H. Hohmann, C. Callegari, S. Furrer, D. Grosenick, E. E. B. Campbell, and I. V. Hertel, Phys. Rev. Lett. **73**, 1919 (1994).

[26] E. E. B. Campbell, K. Hoffmann, H. Rottke, and I. V. Hertel, J. Chem. Phys. **114**, 1716 (2001).

[27] E. E. B. Campbell, K. Hoffmann, and I. V. Hertel, Eur. Phys. J. D **16**, 345 (2001).

[28] F. Rohmund, M. Heden, A. V. Bulgakov, and E. E. B. Campbell, J. Chem. Phys. **115**, 3068 (2001).

[29] E. E. B. Campbell, K. Hansen, K. Hoffmann, G. Korn, M. Tchaplyguine, M. Wittmann, and I. V. Hertel, Phys. Rev. Lett. **84**, 2128 (2000).

[30] V. R. Bhardwaj, P. B. Corkum, and D. M. Rayner, Phys. Rev. Lett. **93**, 043001 (2004).

[31] K. Hansen, K. Hoffmann, and E. E. B. Campbell, J. Chem. Phys. **119**, 2513 (2003).

[32] J. U. Andersen, E. Bonderup, and K. Hansen, J. Phys. B: At. Mol. Opt. Phys. **35**, R1 (2002).

[33] E. E. B. Campbell and R. D. Levine, Annu. Rev. Phys. Chem. **51**, 65 (2000).

[34] J. U. Andersen, C. Gottrup, K. Hansen, P. Hvelplund, and M. O. Larsson, Eur. Phys. J. D **17**, 189 (2001).

[35] K. Hansen and E. E. B. Campbell, J. Chem. Phys. **104**, 5012 (1996).

[36] E. E. B. Campbell and F. Rohmund, Rep. Prog. Phys. **63**, 1061 (2000).

[37] E. E. Campbell, *Fullerene Collision Reactions*, 1st ed. (Kluwer, Dordrecht, The Netherlands, 2003).

[38] K. Hansen, E. E. B. Campbell, and O. Echt, Int. J. Mass. Spectr. **252**, 79 (2006).

[39] M.-A. Lebeault, B. Baguenard, B. Concina, F. Calvo, B. Climen, F. Lepine, and C. Bordas, J. Chem. Phys. **137**, 054312 (2012).

[40] C. Lifshitz, Int. J. Mass Spectr. **198**, 1 (2000).

[41] S. Díaz-Tendero, M. Alcamí, and F. Martín, J. Chem. Phys. **119**, 5545 (2003).

[42] S. Díaz-Tendero, G. Sánchez, M. Alcamí, and F. Martín, Int. J. Mass. Spectr. **252**, 133 (2006).

[43] C. Xu and G. E. Scuseria, Phys. Rev. Lett. **72**, 669 (1994).

[44] T. Kunert and R. Schmidt, Phys. Rev. Lett. **86**, 5258 (2001).

[45] K. Hansen, *Statistical Physics of Nanoparticles in the Gas Phase*, Springer Series on Atomic Optical and Plasma Physics, (Springer, Dordrecht, The Netherlands, 2013).

[46] E. E. B. Campbell, T. Raz, and R. D. Levine, Chem. Phys. Lett. **253**, 261 (1996).

[47] R. Ehlich, M. Westerburg, and E. E. B. Campbell, J. Chem. Phys. **104**, 1900 (1996).

[48] R. Vandenbosch, B. P. Henry, C. Cooper, M. L. Gardel, J. F. Liang, and D. I. Will, Phys. Rev. Lett. **81**, 1821 (1998).

[49] R. Vandenbosch, Phys. Rev. A **59**, 3584 (1999).

[50] S. Díaz-Tendero, M. Alcamí, and F. Martín, Phys. Rev. Lett. **95**, 013401 (2005).

[51] S. Díaz-Tendero, M. Alcamí, and F. Martín, J. Chem. Phys. **123**, 184306 (2005).

[52] H. Zettergren, G. Sánchez, S. Díaz-Tendero, M. Alcamí, and F. Martín, J. Chem. Phys. **127**, 104308 (2007).

[53] H. Cederquist, J. Jensen, H. T. Schmidt, H. Zettergren, S. Tomita, B. A. Huber, and B. Manil, Phys. Rev. A **67**, 062719 (2003).

[54] V. R. Bhardwaj, P. B. Corkum, and D. M. Rayner, Phys. Rev. Lett. **91**, 203004 (2003).

[55] H. Zettergren and H. Cederquist, Phys. Chem. Chem. Phys. **14**, 16770 (2012).

[56] H. Zettergren, H. T. Schmidt, H. Cederquist, J. Jensen, S. Tomita, P. Hvelplund, H. Lebius, and B. A. Huber, Phys. Rev. A **66**, 032710 (2002).

[57] V. Bernigaud, O. Kamalou, A. Ławicki, M. Capron, R. Maisonny, B. Manil, L. Maunoury, J. Rangama, P. Rousseau, J.-Y. Chesnel, L. Adoui, and B. A. Huber, Publ. Astron. Obs. Belgrade **84**, 83 (2008).

[58] T. Bergen, X. Biquard, A. Brenac, F. Chandezon, B. A. Huber, D. Jalabert, H. Lebius, M. Maurel, E. Monnand, J. Opitz, A. Pesnelle, B. Pras, C. Ristori, and J. C. Rocco, Rev. Sci. Instrum. **70**, 3244 (1999).

[59] F. Chandezon, B. A. Huber, and C. Ristori, Rev. Sci. Instrum. **65**, 3344 (1994).

[60] M. Capron, S. Díaz-Tendero, S. Maclot, A. Domaracka, E. Lattouf, R. Maisonny, A. Ławicki, J.-Y. Chesnel, A. Méry, J.-C. Poully, J. Rangama, L. Adoui, F. Martín, M. Alcamí, P. Rousseau, and B. A. Huber, Chem. Eur. J. **18**, 9321 (2012).

[61] M. J. Puska and R. M. Nieminen, Phys. Rev. A **47**, 1181 (1993).

[62] L. F. Ruiz, P.-A. Hervieux, J. Hanssen, M. F. Politis, and F. Martin, Int. J. Quant. Chem. **86**, 106 (2002).

[63] H. Lüdde and R. M. Dreizler, J. Phys. B: At. Mol. Opt. **18**, 107 (1985).

[64] M. F. Politis, P. A. Hervieux, J. Hanssen, M. E. Madjet, and F. Martín, Phys. Rev. A **58**, 367 (1998).

[65] P. A. Hervieux, B. Zarour, J. Hanssen, M. F. Politis, and F. Martín, J. Phys. B: At. Mol. Opt. **34**, 3331 (2001).

[66] C. Bréchignac, Ph. Cahuzac, B. Concina, J. Leygnier, L. F. Ruiz, B. Zarour, P.-A. Hervieux, J. Hanssen, M. F. Politis, and F. Martín, Phys. Rev. Lett. **89**, 183402 (2002).

[67] S. Díaz-Tendero, L. F. Ruiz, B. Zarour, F. Calvo, F. Spiegelman, P.-A. Hervieux, F. Martín, J. Hanssen, and M. F. Politis, Eur. Phys. J. D **44**, 525 (2007).

[68] J. D. Jackson, *Classical Electrodynamics Third Edition*, 3rd ed. (Wiley, New York, 1998).

[69] V. Weisskopf, Phys. Rev. **52**, 295 (1937).

[70] D. H. E. Gross and P. A. Hervieux, Z. Phys. D **35**, 27 (1995).

[71] G. Martinet, S. Díaz-Tendero, M. Chabot, K. Wohrer, S. Della Negra, F. Mezdari, H. Hamrita, P. Désesquelles, A. Le Padellec, D. Gardés, L. Lavergne, G. Lalu, X. Grave, J. F. Clavelin, P. A. Hervieux, M. Alcamí, and F. Martín, Phys. Rev. Lett. **93**, 063401 (2004).

[72] S. Díaz-Tendero, P.-A. Hervieux, M. Alcamí, and F. Martín, Phys. Rev. A **71**, 033202 (2005).

[73] F. Calvo, S. Díaz-Tendero, and M.-A. Lebeault, Phys. Chem. Chem. Phys. **11**, 6345 (2009).

[74] C. Cohen-Tannoudji, B. Diu, and F. Laloë, *Quantum Mechanics* (Wiley, New York, 1977).

[75] A. Reinkoster, S. Korica, G. Prumper, J. Viefhaus, K. Godehusen, O. Schwarzkopf, M. Mast, and U. Becker, J. Phys. B: At. Mol. Opt. **37**, 2135 (2004).

[76] M. Fieber-Erdmann, W. Kratschmer, and A. Ding, Z. Phys. D Atom. Mol. Cl. **26**, 308 (1993).

[77] T. Drewello, W. Krätschmer, M. Fieber-Erdmann, and A. Ding, Int. J. Mass. Spectrom. Ion. Proc. **124**, R1 (1993).

[78] S. Díaz-Tendero, L. F. Ruiz, B. Zarour, J. Hanssen, M. Alcamí, M. F. Politis, P.-A. Hervieux, and F. Martín, J. Phys: Conf. Ser. **194**, 012047 (2009).

[79] A. Rentenier, P. Moretto-Capelle, D. Bordenave-Montesquieu, and A. Bordenave-Montesquieu, J. Phys. B: At. Mol. Opt. **38**, 789 (2005).

[80] H. Lebius, S. Tomita, A. Brenac, F. Chandezon, A. Pesnelle, and B. A. Huber, Phys. Scr. **1999**, 197 (1999).